Carbon 209 (2023) 118009

Contents lists available at ScienceDirect

Carbon

journal homepage: www.elsevier.com/locate/carbon

Separation and online optical characterization of fluorescent components of pyrogenic carbons for carbon dots identification

C. Russo *, A. Ciajolo, F. Stanzione, A. Tregrossi, B. Apicella

Istituto di Scienze e Tecnologie per l'Energia e la Mobilità Sostenibili, STEMS-CNR, Piazzale Tecchio, 80, Napoli, Italy

ARTICLE INFO

Keywords:
Carbon dots fractionation
PAHs
Pyrogenic carbon
Band gap
Quantum yield, Fluorescence

ABSTRACT

Optical features of fluorescent components of pyrogenic carbons as flame-formed carbon particulate matter (PM) were studied by setting up a facile and fast method (SEC-Abs/Fluo) based on size exclusion chromatography (SEC) coupled with UV–Visible absorption and fluorescence spectrometers as detectors. The SEC-Abs/Fluo method simultaneously allowed the molecular weight (MW) separation and identification of blue- and green-fluorescent PM components exhibiting size and spectroscopic features typical of carbon dots (CDs). The SEC-Abs/Fluo method allowed the online determination of quantum yield (QY) and optical band gap of fluorescent components also in strongly-scattering carbon suspensions so avoiding tedious pretreatment of carbon samples. From the detailed separation and analysis of blue- and green-fluorescent PM components along with two commercial pitches, aromatic species having MW > 1000 u and band gap <1–1.5 eV resulted to be scarcely or no fluorescent indicating these are the MW and band gap thresholds for fluorescence emission. Indeed, a sharp QY decrease was for the first time noticed in a narrower band gap (1–1.5 eV) range, where carriers can more easily tunnel to defects of the carbon network reducing fluorescence emission. The exponential increase of QY as the band gap rises was found with a more regular trend for the MW-segregated components in comparison to the bulk samples. The method can support and guide the choice of the optimal operating conditions to maximize CD formation and their purification from not-fluorescing components and can also be helpful in disentangling CD fluorescence attribution.

1. Introduction

Fluorescence is an optical property featuring many kinds of carbon materials like hydrogenated amorphous carbons [1], combustion-formed particulate matter (PM) [2], and peculiar carbons like interstellar carbon dust [3]. Fluorescence is also an important feature of a new class of carbon materials named carbon dots (CDs) coming from diverse top-down and bottom-up processes involving single organic species and/or materials like biomasses, graphite, and carbon nanotubes. Due to their fascinating properties and possible applications, a plethora of scientific works has been devoted to the study of CDs [4–8]. Low toxicity, high biocompatibility and chemical stability [9,10] make CDs a promising alternative to semiconductor quantum dots and organic dyes for applications in various fields, from imaging to sensing, photocatalysis, and energy conversion [11–15]. Hence, research efforts have been devoted both to understand the fluorescence origin and to look for reliable top-down and bottom-up methods for scalable and controllable synthesis of CDs [16].

Top-down processes involve harsh physical and chemical treatments like the exfoliation and oxidation of carbon materials and are so based on laborious approaches as laser and chemical ablation [17], arc discharge [18] and plasma sources [19]. Bottom-up approaches encompass more facile synthesis routes, including hydrothermal or solvothermal carbonization [20,21], acid hydrolysis [22], flame synthesis [23–27] and, microwave pyrolysis [28], starting from low-toxic organic compounds or natural materials as biomasses or waste-derived sources. Bottom-up processes for CD production generally involve dehydration/carbonization or polymerization/self-assembly of specific molecular organic precursors, e.g., citric acid and polycyclic aromatic hydrocarbons (PAHs). Citric acid is the most popular source for producing CDs of high quantum yields (QYs) by bottom-up methods involving dehydration and carbonization [13–16]. Low molecular weight (MW) hydrocarbons like PAHs are instead precursors involved in an easily-accessible bottom-up process based on hydrocarbon combustion in partially oxidative conditions forming multiemissive nanocarbon sources like candle soot [26,29], as-formed lamp [30] and in-flame soot

* Corresponding author.
E-mail address: carmela.russo@stems.cnr.it (C. Russo).

https://doi.org/10.1016/j.carbon.2023.118009
Received 16 February 2023; Received in revised form 7 April 2023; Accepted 8 April 2023
Available online 10 April 2023

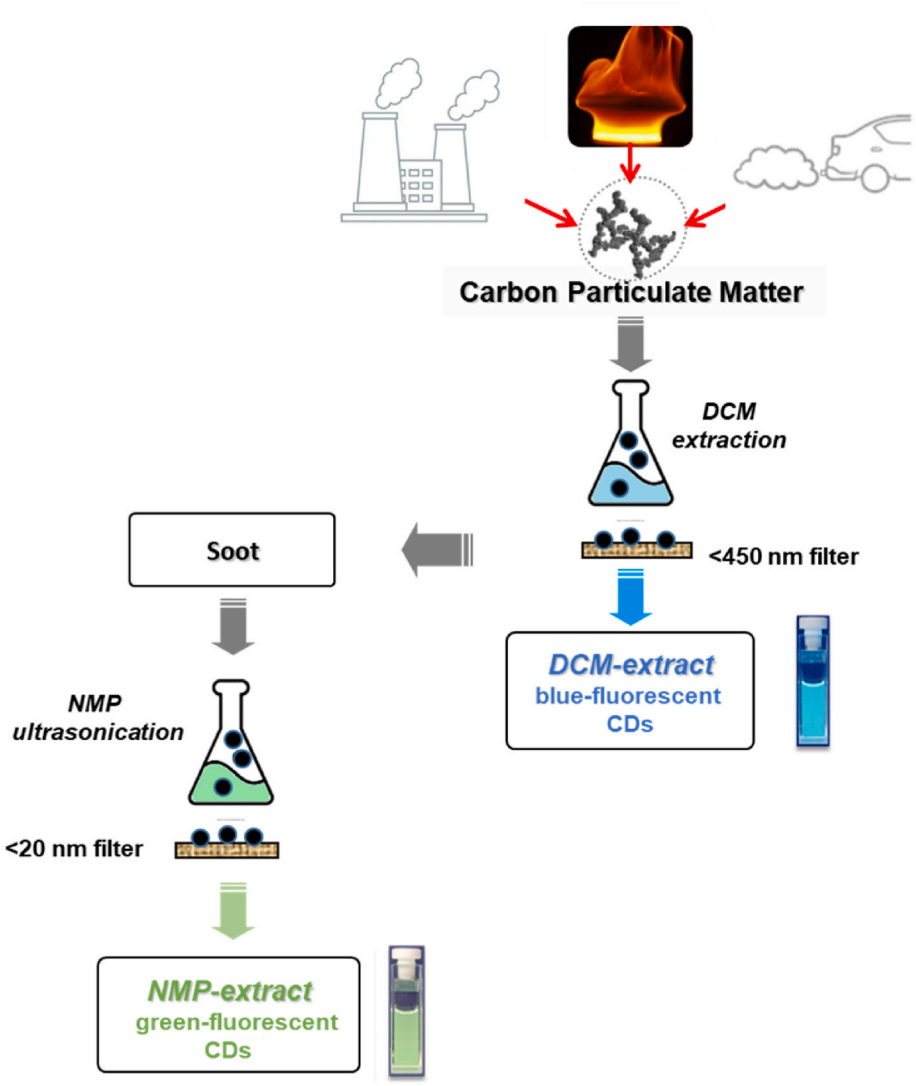

Fig. 1. Separation scheme of carbon PM. (A colour version of this figure can be viewed online.)

samples [23–25,31–33]. The composition of the reaction mixture decisively influences the formation of carbonaceous species [25] that is closely related to the lack of oxygen in the reactive processes. The most common parameter used to describe a fuel/air mixture is the equivalence ratio φ, defined as the ratio of the real fuel-to-oxidizer ratio to the stoichiometric fuel-to-oxidizer ratio. In fuel-rich conditions ($\varphi > 1$) fuel fragments tend to form heavier compounds and eventually carbon nanoparticles.

Whichever the source and the kind of CD production process, the formation of multicomponent mixtures with a high level of impurities is generally observed, which make difficult the correct attribution and interpretation of fluorescence mechanisms [34] and the safe application of CDs in specific fields like biomedicine. As matter of fact the fluorescence attribution for CDs is very debated and three main emission mechanisms are generally considered [35]: i) the surface states emission, related to the presence of functional groups connected with the carbon backbone [36,37]; ii) the core emission, due to the conjugated π-domains of carbon core or to the quantum confinement effect [38,39]; and iii) the molecular state emission, originating from free or bonded fluorescent molecules [40,41]. Actually, the conjugation of π–π domains [36] is one of the mechanisms proposed for interpreting the fluorescence of CDs, especially of those having few surface functional groups, for which the emission center lies in the carbon core and is determined by the band gap of conjugated π-domains [42]. Typical examples of species with aromatic conjugated moieties are PAHs considered the species useful for mimic optical properties of CDs [8] as well as precursors of some carbon materials derived from pyrogenic processes [2]. The difficulties in CD fluorescence attribution are also due to the persistence of molecular precursors of CDs (citric acid, PAHs and so on), and of byproducts or molecular scaffolds that could significantly contribute to the mixture fluorescence [23,43–45]. Their presence cannot be detected by transmission electron microscopy (TEM), largely employed for determining another critical property of CDs, i.e., their size [46]. Consequently, and also because of the possible interference of non-fluorescent carbon material, separation and purification methods are obliged passages for improving CD production and application, and for studying their fluorescence mechanisms.

Size exclusion chromatography (SEC) performed on a high pressure liquid chromatography system allows to rapidly separate classes of carbon components in order of decreasing MW/size. The fractions can be recovered downstream of the SEC system and analyzed for individuating the fluorescent and non-fluorescent components [47–50]. However, the collection of specific MW/size-segregated fractions requires a careful evaluation of the elution time and is particularly crucial when chromatographic peaks are not well separated and partially overlapped. Furthermore, the fractions recovered from SEC column are very diluted so that multiple injections are necessary to collect enough specimen to be further analyzed [51]. Additionally, the use of low-volatile eluents

Table 1
List of analyzed samples with source description.

Samples	Description
Flame-generated samples	
Soot	DCM-insolubles of carbon PM sampled in an ethylene laminar premixed flame
Blue CDs (DCM-extract)	DCM-extract of carbon PM sampled in an ethylene laminar premixed flame
Green CDs (NMP-extract)	NMP-extract of soot filtered on 20 nm filter
PAH-laden samples	
Aromatic pitch 1 (ArP1)	Electrode binder pitch (Rutgers): 65996-93-2
Aromatic pitch 2 (ArP2)	Carbores (Rutgers): 121575-60-8

makes difficult sample fraction recovery by solvent evaporation.

Our previous work reports about the fluorescence emission of species extracted from carbon PM due to molecular fluorophores like PAHs, π-conjugated aromatic domains and carbon-core states [23,52]. The attribution of fluorescence to specific components and the evaluation of their optical properties have been done in the present work setting up a rapid method based on SEC coupled with UV–Visible absorption and fluorescence spectrometers as detectors (SEC-Abs/Fluo) able to achieve the simultaneous estimation of the MW distribution and the online spectroscopic analysis of the main components of carbon PM. The procedure has been implemented on flame-formed carbon PM composed of soot and blue- and green-fluorescent components extracted from PM as schematized in Fig. 1. Meaningful spectroscopic properties as optical band gap and quantum yield (QY) have been evaluated analyzing the online UV–Visible (UV–Vis) absorption and fluorescence spectra acquired at selected MW as described in section 3.1. Absorbance and fluorescence chromatograms and online spectroscopic features of soot and green-fluorescent CDs separated on a wide-MW range column are reported in Sect. 3.2. Details on blue- and green-fluorescent CDs, separated in a narrower MW range on a different column, are described in section 3.3. Spectroscopic data are analyzed in sect. 3.4, with particular regard to the optical band gap and QY features, also in reference to the analysis of commercial pitch samples.

2. Experimental

2.1. Samples and preparation procedure

Carbon PM was thermophoretically sampled from a heavily-sooting premixed ethylene/oxygen flame (at 8 mm above the burner and $\varphi = 3.0$) [53] on a rotating glass plate driven by a gear motor. Carbon PM caught on the plate was submitted to a separation procedure schematized in Fig. 1. It was first treated with dichloromethane (DCM) and then filtered on Teflon filters (0.45 μm pore size, Millipore) for separating the insoluble solid phase, here named soot, from the DCM-extract. Stable suspensions of soot recovered from the Teflon filter were obtained by ultrasonic stirring in N-Methyl-2-Pyrrolidone (NMP). Soot suspensions were filtered on 0.02 μm membrane filters (Anodisc) separating solid particles with diameter >20 nm from components transferred into the NMP-extract. DCM- and NMP-extracts showed to emit fluorescence in the blue and green region, respectively [23]. On the basis of their spectroscopic properties, along with SEC and TEM analysis [23] demonstrating their nanometric/subnanometric size, the DCM- and NMP-extracts have been here named as blue- and green-fluorescent CDs, respectively. More experimental details on the sampling and separation procedure are reported in previous works [23,54].

Benzo(ghi)perylene, anthracene and 9,10-diphenyl anthracene, used as standards to set up and verify the SEC-Abs/Fluo method, were obtained from Sigma Aldrich. Coal tar pitches named aromatic pitch 1, ArP1 (Electrode binder pitch: 65996-93-2 [55]) and aromatic pitch 2, ArP2 (Carbores: 121575-60-8 [55]), kindly provided by Rain Carbon Inc., were also analyzed as typical mixtures of unsubstituted PAHs, which are strongly absorbing and fluorescing in the UV–Vis wavelength range [55]. Carbon PM and pitches studied in this work are mainly composed of carbon and hydrogen atoms with a negligible presence of nitrogen and oxygen as derived from elemental analysis and confirmed by infrared spectroscopy [55–57]. Table 1 reports the list of carbon samples here analyzed.

2.2. Sample separation and spectroscopic characterization methods

Standard PAHs (benzo(ghi)perylene, anthracene and 9,10-diphenyl anthracene), pitches and as-prepared carbon samples (soot, blue-fluorescent CDs (DCM-extract) and green-fluorescent CDs (NMP-extract)) were dissolved/suspended in NMP and analyzed by steady-state UV–Vis absorption and fluorescence spectroscopy. Steady-state UV–Vis absorption spectra were measured on a HP8453 spectrophotometer in standard 1 cm path-length quartz cells (samples concentration 10 mg/l) whereas steady-state fluorescence spectra ($\lambda_{exc} = 350$ nm) were measured in standard 1 cm path-length quartz cells on a HORIBA Scientific FluoroMax-Plus TCSPC spectrofluorometer (sample concentration 0.1–1 mg/l).

SEC-Abs/Fluo analysis of NMP suspensions of soot and green-fluorescent CDs separated from soot by extraction with NMP and filtration, was carried out on a HPLC system HP1050 series using a Jordi Gel DVB Solid Bead column 300 × 7.8 mm for the MW determination in a wide range, namely 2000–10^11 u range. The injection volume was 10 μl, NMP was used as eluent at room temperature with a flow rate of 0.8 ml/min. Soot suspended in NMP was injected at a concentration of 100 mg/l whereas the concentration of green-fluorescent CDs was estimated to be around 20 mg/l by gravimetric measurements of soot deposited on the Anodisc filter. The absorbance and fluorescence chromatograms of standard species and samples were simultaneously obtained by placing in series at the exit of the SEC column an UV–Vis absorption and a fluorescence spectrometric detector. Specifically, the absorption chromatogram was obtained by fixing the absorption wavelength at 350 nm, of an HP1050 UV–Vis diode array detector able to simultaneously measure the absorption spectra in the whole 250–600 nm wavelength range. The fluorescence chromatogram was obtained by fixing the excitation and emission wavelength ($\lambda_{exc} = 350$ nm, $\lambda_{em} = 500$ nm) of a G1321AR fluorescence detector able to measure fluorescence spectra in the 280–900 nm emission range selecting the excitation wavelength in the 200–700 nm range. The online absorption and fluorescence spectra were acquired in the 250–600 nm and in the 375–600 nm absorption and emission wavelength range, respectively. On the basis of standard PAH analysis, a delay time of 0.1 min between absorbance and fluorescence chromatograms was evaluated. The fluorescence chromatograms have been accordingly back shifted to allow the direct comparison of the chromatograms and evaluate the QY by dividing the absorption and fluorescence signals for selected MW, as detailed in the result section.

The MW separation/determination of blue- and green-fluorescent CDs was also carried out in a narrower MW range (100–10^5 u) on a highly cross-linked "individual-pore" column (Polymer Laboratories, Ltd., U.K.; particle size of 5 μm diameter and a pore dimension of 50 nm). In this case the injection volume was 100 μl and the analyses were performed at a temperature of 70 °C with a flow rate of 0.5 ml/min using sample concentrations around 10–20 mg/l.

On both SEC columns the MW calibration was obtained by determining the retention time of polystyrene and PAH standard species of known MW [58] and soot particles with known size as derived by dynamic light scattering, assuming a spherical particle shape and a density of 1.8 g/cm^3 [59]. On the basis of these standard species the retention time abscissa of the SEC profiles reported in the paper were transformed

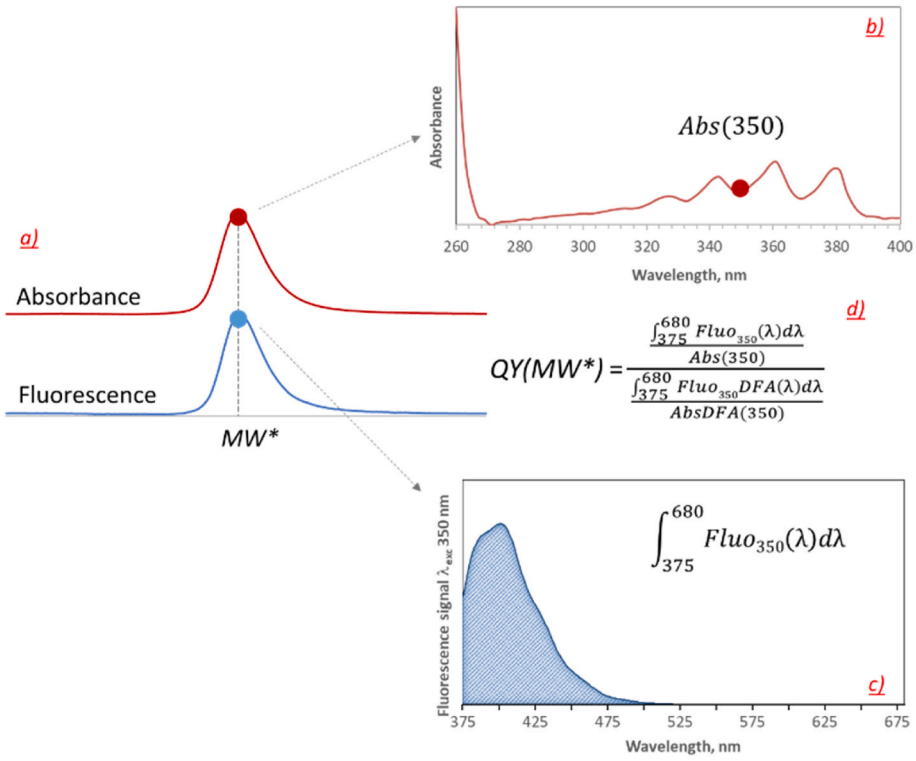

Fig. 2. Exemplificative chromatograms of an individual species detected by absorption (λ_{abs} = 350 – red curve) and fluorescence (λ_{exc} = 350 nm, λ_{em} = 500 nm – blue curve) chromatograms (a). Absorption (b) and fluorescence (λ_{exc} = 350 nm) (c) spectra at a selected MW. The formula used for QY evaluation at a specific MW of the chromatograms is reported in (d). (A colour version of this figure can be viewed online.)

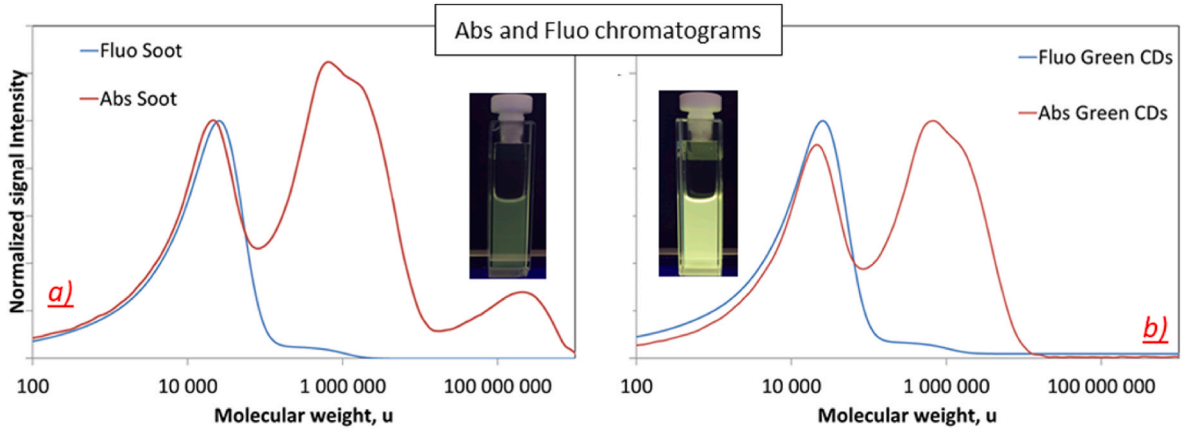

Fig. 3. Absorption (λ_{abs} = 350) and fluorescence (λ_{exc} = 350 nm, λ_{em} = 500 nm) chromatograms of soot (a) and green-fluorescent CDs (b) as a function of MW. In the inset, the images of the samples in NMP solution under UV light (λ_{exc} = 365 nm). (A colour version of this figure can be viewed online.)

in MW.

3. Results and discussion

3.1. Online evaluation of QY and optical band gap of SEC-separated carbon fractions

The SEC-Abs/Fluo method simultaneously gives out an absorption and a fluorescence chromatogram as those shown in Fig. 2a, where exemplificative chromatograms of a single fluorescent species are reported.

The optical band gap values have been evaluated on the UV–Vis absorption spectra measured at selected MW of the absorption chromatograms applying the Tauc method [59–61] proposed in early work for deriving the band gap energy of germanium, i.e., the energy gap between the conduction and valence band, using its optical absorption spectrum. It has been found that the absorbance A follows the Tauc relationship: $A * E = B * (E - E_g)^r$, where E is the energy of the incident radiation, B is a constant, E_g is the optical band gap and r is a constant varying according with the reciprocal values of the moment of the top of the valence band and of the bottom of the conduction band energy. The Tauc equation has been used for calculating the band gap of amorphous carbons as carbon PM imposing a r value of 2: if (AE)ˆ(1/2) vs E is a straight line, E_g can be obtained from the extrapolation to energy axis. On the basis of the sp^2-bonded cluster model proposed by Robertson and O'Reilly [61], the size of sp^2−bonded clusters, i.e., the aromatic layer length usually named L_a, can be derived according to the formula E_g (eV) = 7.7/L_a.

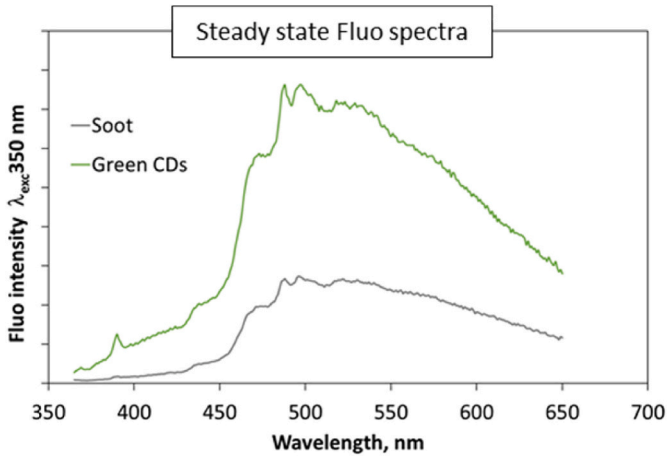

Fig. 4. Steady-state fluorescence spectra (λ_{exc} = 350 nm) of soot suspension and green-fluorescent CDs. (A colour version of this figure can be viewed online.)

For the determination of QY, a reference species with unitary QY, namely 9,10-diphenyl anthracene (DFA) [62], was injected into the SEC system. It produced one single peak in the chromatograms obtained by absorption and fluorescence detection at fixed wavelengths. Actually, the detectors allow the online measure of absorption and fluorescence spectra, respectively, which can be measured, point by point, on the chromatograms. Exemplificative absorption and fluorescence spectra are reported in Fig. 2b and c, respectively, along with the formula used for QY evaluation (Fig. 2d). At a specific MW (MW*) the integrated area of the fluorescence spectrum produced by excitation at a fixed wavelength (350 nm) was divided by the absorbance value at the same wavelength. This emission/absorption ratio was then divided by the same ratio measured for the DFA reference species in order to evaluate the QY of the MW-segregated components of carbon samples. The QY values of single standard PAHs, namely benzo(ghi)perylene and anthracene, were evaluated applying the same method on the chromatographic peaks obtained by SEC injection and compared with the QY measured using steady-state fluorescence and absorption spectra. The QY of these PAHs evaluated on online and steady-state fluorescence spectra resulted to be very similar (0.31 and 0.28 for benzo(ghi)perylene, and 0.34 and 0.38 for anthracene), supporting the reliability of the online QY evaluation method.

3.2. Soot and green-fluorescent CDs: SEC separation on a wide-MW range and spectroscopic analysis

Soot is typically constituted of carbon species distributed in a very wide MW/size range, going from strongly-adsorbed and/or imbedded organic carbon components of relatively high MW (300-1000 u) [63], up to solid carbon particle/aggregates with MW around 10^9 u, roughly corresponding to aggregate size of about 100 nm [59]. The chromatograms in a such wide MW of soot and green-fluorescent CDs (Fig. 1) have been obtained on a wide-MW range column (sect. 2.1) simultaneously registering absorption and fluorescence signals collected at appropriate absorption wavelength (λ_{abs} = 350 nm) and fluorescence wavelengths (λ_{exc} = 350 nm and λ_{em} = 500 nm).

The absorption (red lines) and fluorescence (blue lines) chromatograms of soot and of green-fluorescent CDs, are reported in Fig. 3a and b, respectively, as a function of the MW.

On the basis of standard samples (see Sect. 2.2) different MW/size-segregated classes could be assigned to the chromatographic peaks [59]. The last peak of the soot absorption chromatogram is ascribed to particles/aggregates of 100 nm (Fig. 3a), whereas the first and second peaks can be attributed to single 5–20 nm soot particles and compounds with MW falling in the range 100–10^5 u, respectively [59]. Only these two latter peaks are noticed in the absorption chromatogram of green-fluorescent CDs (red line in Fig. 3b), whereas the 100 nm aggregate peak is obviously absent because green-fluorescent CDs derive from filtration on 20 nm membrane filters (Fig. 1) blocking particles/aggregates having size >20 nm. Consistently with the absence of 100 nm particle aggregates, scattering visually observed in the image of soot suspension (inset of Fig. 3a) is quite absent in the image of green-fluorescent CDs (inset of Fig. 3b). The scattering and reabsorption of the incident and/or emitted radiation by these particle aggregates reduce the fluorescence emission of soot, but do not modify its spectral shape as shown in Fig. 4 displaying the comparison of the steady-state fluorescence spectra (λ_{exc} = 350 nm) of soot and green-fluorescent CDs with the same fluorophore concentration.

The comparison of absorption and fluorescence chromatograms clearly shows that both the aggregates and small soot particles do not present significant fluorescence (Fig. 3a). Specifically, the fluorescence chromatogram of both soot and green-fluorescent CDs (blue lines in Fig. 3a–b) exhibits only one peak corresponding to compounds with a MW in the range 100–10^5 u that falls at the lower limit of MW linearity for the column used.

The optical band gap values of soot and green-fluorescent CDs have been evaluated on the UV–Vis spectra measured on the peaks of absorption chromatograms (red lines of Fig. 3a and b). The optical band gap values of 0.27 and 1.17 eV were evaluated on the UV–Vis spectra measured on the aggregates and particles peaks, respectively. These

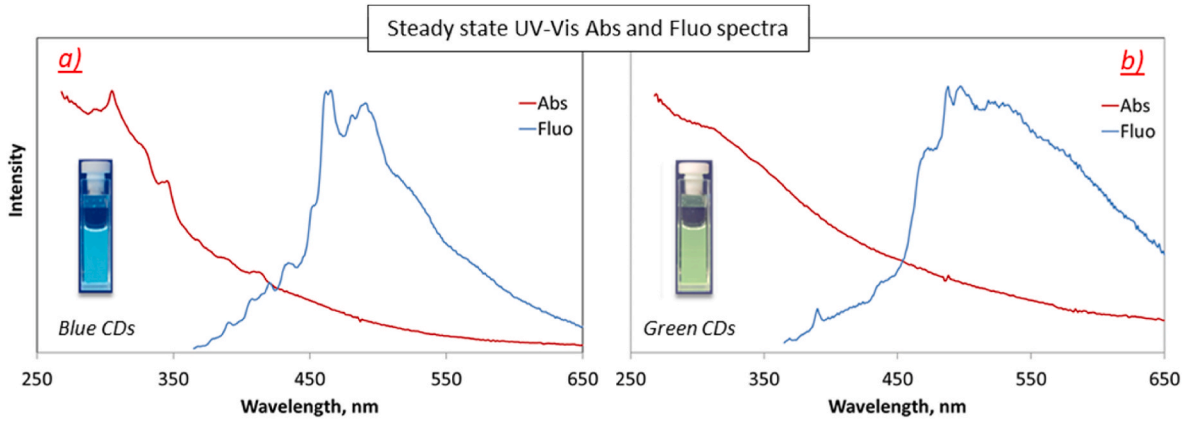

Fig. 5. UV–Vis absorption and fluorescence (λ_{exc} = 350 nm) spectra of blue-fluorescent (a) and green-fluorescent CDs (b). (A colour version of this figure can be viewed online.)

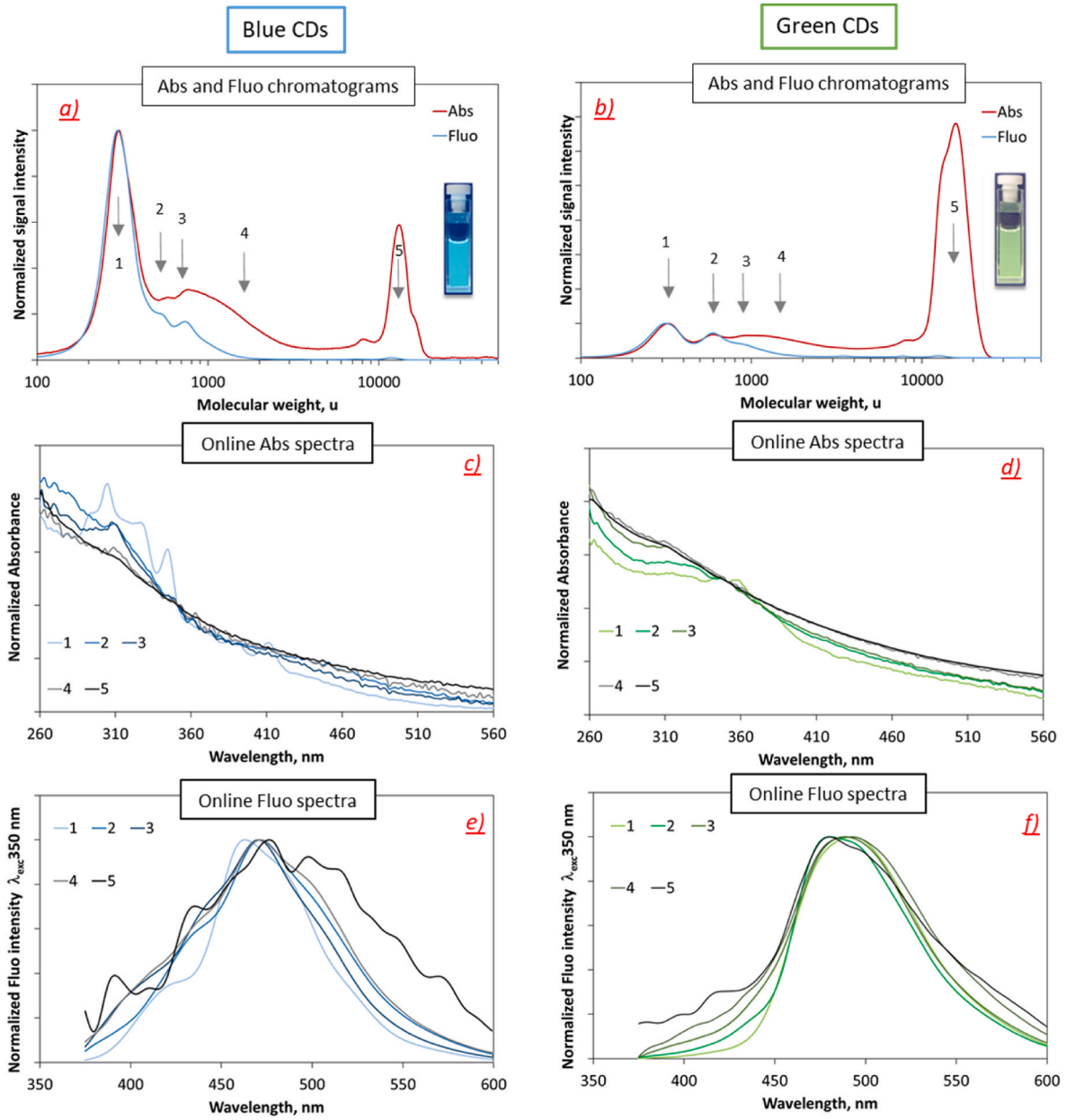

Fig. 6. Absorption ($\lambda_{abs} = 350$) and fluorescence ($\lambda_{exc} = 350$ nm, $\lambda_{em} = 500$ nm) chromatograms of blue-fluorescent (a) and green-fluorescent CDs (b) as a function of MW. Arrows numbered 1 to 5 indicate the points where online absorption (c, d) and fluorescence (e, f) spectra have been collected. The inset in a) and b) report the images of the blue- and green-fluorescent samples in NMP solution under UV light (365 nm). (A colour version of this figure can be viewed online.)

values lie in the range typical of particles, while a higher optical band gap (1.52 eV) features the smaller and more fluorescent components [64]. Interestingly, quite similar optical band gap values, namely 1.19 and 1.64 eV, could be evaluated on the two corresponding peaks of the absorption chromatographic profiles of green-fluorescent CDs (Fig. 3b). Likewise, the QY values of both soot and green-fluorescent CD chromatograms, evaluated for the species eluting as unique peak in the fluorescence chromatograms (blue lines of Fig. 3a and b), resulted to be very similar, namely 8.2 and 8.6%, respectively. The QY measured for soot suspension was 0.4% completely hiding this valuable fluorescent component due to the presence of soot particles quenching fluorescence emission.

The similarity of the online optical properties of soot and green-fluorescent CD components demonstrates that, beside the MW estimation, the SEC-Abs/Fluo method allows the online determination of optical band gap and QY of fluorescent components directly in strongly-scattering suspensions of solid carbons like soot, without need of any further filtration or purification steps. It is also noteworthy that only one class of species of relatively low MW resulted to be responsible of soot green-fluorescence indicating that species above this MW range cannot emit fluorescence in spite of their aromatic character testified by UV–Vis absorption. Interestingly, the transfer of green-fluorescent CDs species in the NMP-extract left behind non-fluorescent soot particles aggregates which could no longer be effectively re-suspended. This indicates that green-fluorescent CDs constitute a sort of "glue" for soot particles as having hydrogen functionalities that give to soot fluorescing properties and allow their dispersion in organic solvents.

It is worth to note that the main fluorescent component of green-fluorescent CDs has MW close to the MW of light blue-fluorescing PAH molecules, formerly removed from carbon PM by DCM extraction (Fig. 1) [23,33,63]. To improve the MW estimation getting in-depth insights on their spectroscopic features, both blue- and

Table 2
Optical band gap and QY of pitches, CDs and of relative MW-segregated fractions (see rows in Fig. 6 and Fig. S1). MW as evaluated from SEC analysis and the MW of the aromatic unit mass as derived from optical band gap are also reported.

Sample	Band gap, eV	QY, %	MW, u (by SEC analysis)	MW, u (by band-gap equation [59-60])
Green CDs bulk	**1.27**	**3.26**		
Green CDs (1)	1.68	12.7	326	437
Green CDs (2)	1.56	8.13	617	494
Green CDs (3)	1.53	2.77	888	510
Green CDs (4)	1.3	0.3	1400	671
Green CDs (5)	1.2	0.11	16337	770
Blue CDs bulk	**1.72**	**13.78**		
Blue CDs (1)	1.98	15.57	295	335
Blue CDs (2)	1.8	11.91	514	391
Blue CDs (3)	1.84	9.03	707	377
Blue CDs (4)	1.62	1	1679	464
Blue CDs (5)	1.42	0.44	13013	578
ArP1 bulk	**1.57**	**20.26**		
ArP1 (1)	2.06	30.98	312	315
ArP1 (2)	1.73	15.77	849	417
ArP1 (3)	1.59	6.52	1338	479
ArP1 (4)	1.21	0.53	12434	758
ArP2 bulk	**1.45**	**16.32**		
ArP2 (1)	2	29.36	564	330
ArP2 (2)	1.53	5.36	1115	510
ArP2 (3)	1.49	2.46	1338	533
ArP2 (4)	1.28	0.23	12434	689

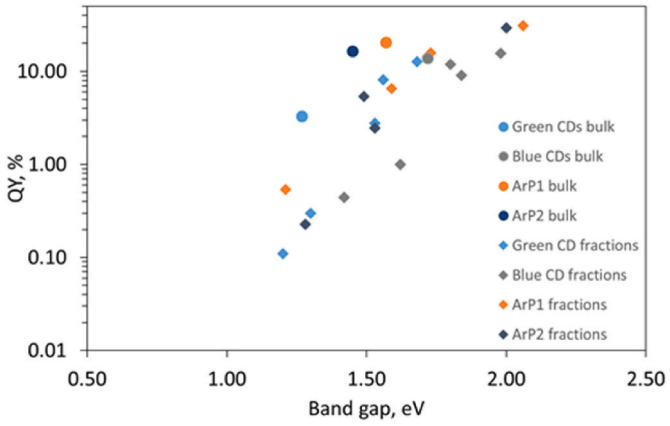

Fig. 7. QY as a function of optical band gap as evaluated on the spectra of the bulk spectra (circles) of pitches and CDs and on their relative MW/size segregated fractions (diamonds). (A colour version of this figure can be viewed online.)

green-fluorescent PM components have been further analyzed on a SEC column able to separate them in a narrower MW range, down to 100 u (Sect. 2.1).

3.3. Blue- and green-fluorescent CDs: MW distribution and spectroscopic features

Before of describing the detailed SEC separation and spectroscopic analysis of blue- and green-fluorescent CDs derived from carbon PM, some observations can be done on their steady-state spectroscopic properties.

UV–Vis absorption and fluorescence (λ_{exc} = = 350 nm) spectra of blue-fluorescent CDs are reported in Fig. 5. The fine structure of the UV–Vis absorption spectrum (Fig. 5a) and a broad fluorescence emission in the 360–600 nm wavelength region peaked at 470–480 nm (Fig. 5b) hint to the large PAH abundance in the blue-fluorescent CDs as also confirmed by the high QY (13.7% at λ_{exc} = 350 nm) typical of small-medium size PAHs [62]. Green-fluorescent CDs present a structureless absorption spectrum and a fluorescence spectrum shifted and broadening toward higher wavelengths (Fig. 5b), along with a relatively low QY (3% at λ_{exc} = 350 nm). These features are typical of relatively large PAHs (MW > 300 u) either in form of planar or curved PAHs [33,63,65].

Fig. 6 reports the absorption and fluorescence chromatographic profiles of blue- (Fig. 6a) and green-fluorescent CDs (Fig. 6b) obtained on the species eluting in the 50000 down to 100 u MW range. The overall improvement of the separation can be seen by comparing the chromatographic profiles obtained on the two columns of green-fluorescent CDs (cfr. Figs. 3b and 6b). As matter of fact, the chromatographic profiles of Fig. 6b show that the low-fluorescing species are much better separated from the fluorescent ones. Moreover, green-fluorescent species, appearing as a unique peak on the wide-MW column (Fig. 3b), are further separated in form of a major peak at 300 u with a broad shoulder due to species with MW ranging from 500 to 2000 u (Fig. 6b).

The absorption chromatograms of both blue- and green-fluorescent CDs (red lines in Fig. 6a and b) shows three main peaks corresponding to three MW-segregated fractions centered around 300, 800 and 10000-20000 u, respectively [33,50,58]. However, some remarkable differences can be observed in the relative peak intensity. The peak corresponding to 200-600 u species is predominant for blue-fluorescent CDs, especially in comparison to the adjacent shoulder associated to species h a MW of 600–1000 u (Fig. 6a). This inference is consistent with the predominance of small planar PAHs also inferred from the fine-structure of blue-fluorescent CD absorption spectrum (Fig. 5a). Green-fluorescent CDs present a more uniform and similar intensity distribution of the two peaks in the 200-1000 u range whereas the third peak, in the 10000-20000 u MW range, is clearly prevalent (Fig. 6b).

It can be seen that only the low-MW species, up to about 1000 u, present significant fluorescence emission so that 1000 u seems a sort of MW threshold for emitting fluorescence from this kind of carbon species.

Fig. 6 displays the UV–Vis absorption and fluorescence spectra (λ_{exc} = 350 nm) measured at different MW for blue- and green-fluorescent CDs. The fine structure of the UV–Vis absorption spectrum of species having MW peaked at 300 u is particularly evident for blue-fluorescent CDs and appears to be broadened as the MW increases (Fig. 6c).

In comparison to blue-fluorescent CDs, green-fluorescent species exhibit broader and less structured absorption spectra (Fig. 6d) and fluorescence spectra shifted toward longer emission wavelengths consistently with their emission into the green. The online fluorescence spectra of green-fluorescent CDs do not show significant spectral changes with the MW increase (Fig. 6f).

The different features of fluorescent components have been deeply analyzed in the following section focused on the spectroscopic parameters, namely the optical band gap and QY, evaluated at different MW values for blue- and green-fluorescent CDs.

3.4. QY and optical band gap analysis

The QY and optical band gap of blue and green-fluorescent samples and their SEC-separated fractions are reported in Table 2 in comparison with those evaluated on fluorescent commercial samples typically containing PAHs like aromatic pitches [55]. Beside their PAH character, these pitches have been chosen as showing SEC profiles, reported in Fig. S1 (supplementary material), peaked in a MW range similar to that of blue- and green-fluorescent CDs. It is interesting to note that pitches present a broad peak in the 200-1000 u region hinting to a wide MW distribution of species of similar structure [55], whereas the main fluorescing components of blue-and green-fluorescent CDs (blue lines in

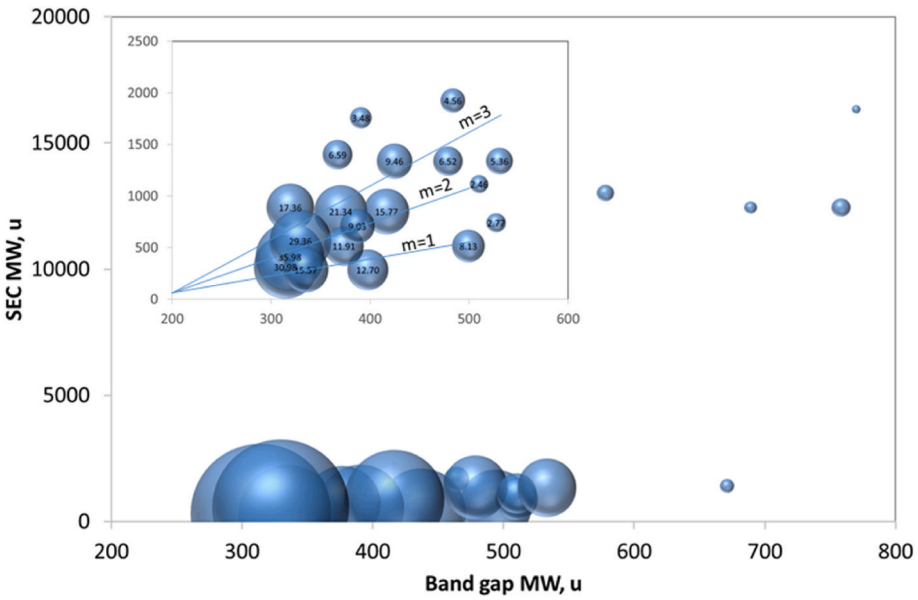

Fig. 8. MW as derived from SEC analysis as a function of the MW of aromatic mass unit as derived from the optical band gap at selected chromatographic points of pitches and CDs. A zoom for MW up to 2500 u and for aromatic mass unit up to 600 u is reported along with three straight lines having 1, 2 and 3 slope (m) values. QY values are reported inside the bubbles of the inset. (A colour version of this figure can be viewed online.)

Fig. 6) elute as two rather distinct fractions: a predominant fraction in form of a sharp peak centered at low MW, below 300-400 u, and a minor fraction in correspondence of a broad shoulder at higher MW. This inference has suggested the occurrence of a structural change as the MW of PAHs increases above 300-400 u like the change from planar PAHs, featuring the major peak, toward curved cyclopenta-PAHs as MW increases [63]. Indeed, such structural change is somehow expected in the growth of PAH beyond 300-400 u at high-temperature conditions and in flames carried out in fuel-rich conditions [66].

The relationship between the band gap and QY before observed for amorphous carbon [67] has been found to occur also for carbon PM and pitches. In particular, in this work for the first time we have analyzed the variation of PL in a wider range of optical band gap, including values down to 1.2 eV.

Particularly, a broad trend of increasing QY with the optical band gap rise is well evidenced in Fig. 7 showing the exponential increase of QY as the band gap rises. Noteworthy, QY values of the unseparated bulk samples lie a little bit out from the regular broad trend demonstrating the need of isolating the fluorescent species from a complex carbon matrix for a proper determination of their properties. In this regard, the SEC-Abs/Fluo method, and in particular the online determination of optical properties on the MW-segregated peaks, appears a good approach for determining these properties avoiding preliminary filtration of carbon PM. It can be also noticed that the QY strongly decreases in correspondence of very low values of band gap (1–1.5 eV), as typically occurs for narrow optical band gap hydrogenated amorphous carbons [67], where carriers can more easily tunnel to defects of the carbon network reducing fluorescence emission.

Interestingly, these low band gap values correspond to MW around 1000 u as estimated by applying the empirical relation between the optical band gap and the MW of the polyaromatic basic unit also reported in Table 2 [61]. This relationship is strictly valid for planar and pericondensed PAHs, since band gap is also affected by the distortion induced by rings or chains and ring arrangement. Studying carbon nanoparticles produced by pulsed-laser pyrolysis of hydrocarbons Llamas-Jansa et al. [68] highlighted the disagreement between the Tauc-derived and HRTEM-measured size of aromatic clusters, confirming the inappropriateness of the model to provide quantitative information on the internal structure of complex and disordered carbon materials. Indeed, DFT calculations have demonstrated that cross-linking, curvature, symmetry, and radical character have an impact on optical band gap values [69]. Moreover, also the high sp^2 concentration of sp^2-rich high-density amorphous carbon as soot [64] prevents any clusters from being independent each other and the interaction between π-systems in the solid state reduces the band gap [64,70]. Overall, it is confirmed that the optical band gap determination is a reliable method to evaluate the MW only for small aromatic systems [70] and the comparison of MW evaluated by SEC and optical band gap (Table 2) confirms that this relationship can be used just to get MW from the lighter fluorescent components of blue- and green-fluorescent CDs.

Moreover, being the optical band gap sensitive to the size/MW of aromatic moieties, it can be deduced that heavier and less fluorescent components are constituted of aggregates of PAHs. The probability of non-radiative decay for PAH aggregates is higher causing the decrease of QY [71]. This aspect is clearly visible in the bubble diagram reported in Fig. 8 where for selected MW fractions (Table 2) the MW values of fluorescing species estimated from the SEC analysis, named SEC-MW, are plotted versus the MW of the aromatic unit, named band gap-MW, whose size has been derived by the band gap using the cluster model [61]. In the inset reporting SEC-MW up to 2500 u also straight lines with slopes (m) going from 1 to 3 are reported. It can be seen how the size of the bubble, indicative of the QY magnitude, is larger for species having low MW whatever the evaluation method is used. Moreover, the bubble size decreases as soon as the SEC-MW overcomes the band gap-MW, namely when SEC-MW becomes two-three times the band gap-MW. The higher values of QY are mainly enclosed between the straight lines corresponding to m = 1 (SEC-MW = Band-Gap MW) and m = 3 (SEC-MW = 3*band gap-MW). Further decrease of QY occurs for larger SEC-MW values and this inference along with the difference between the SEC- and band gap-MW support the attribution of high-MW species to PAH aggregates. As the aromatic unit size increases exceeding a certain size (400-500 u), aromatic molecules rapidly coagulate to form large poorly fluorescent aggregates.

4. Conclusions

This study represents the first investigation on the separation and simultaneous estimation of MW and optical properties, namely spectral

features, optical band gap and QY, of fluorescing and not-fluorescing components of carbon particulate matter. A fast method (SEC-Abs/Fluo) involving SEC coupled with online UV–Vis absorption and fluorescence spectrometers, proved to be able to easily measure the MW distribution and UV–Vis absorption and fluorescence spectral properties of MW-segregated species present also in strongly-scattering carbon suspensions without the need of filtering and separating them by solvent extraction. In view of the renewed interest in the fluorescent properties of carbonaceous materials as possible CD sources, the method represents an innovative, rapid and simple analysis for a deep and detailed characterization of fluorescing components.

It was also shown as the SEC-Abs/Fluo method can be used as a rapid screening tool for analyzing, with just one measurement, CD-containing carbon materials to.

- individuate the fluorescent MW/size -segregated fractions,
- directly evaluate the optical properties of the fluorescent components along all the MW/size distribution featuring CDs.

Specifically, optical parameters, as the optical band gap and the QY, important for evaluating CD performance, could be online evaluated on size/MW segregated components as a function of the MW. The exponential increase of QY as the band gap rises was found with a more regular trend for the MW-segregated components in comparison to the unseparated bulk sample. Moreover, for the first time we have analyzed PL in a wider range of optical band gap, including values down to 1.2 eV.

The method can support and guide both the choice of the optimal operating conditions to maximize CD formation and the search for the better solvent able to purify/isolate fluorescing from not-fluorescing components. Moreover, this analysis easily distinguishes and individuates the molecular fluorophores often widely spread in synthesized CDs.

CRediT authorship contribution statement

C. Russo: Conceptualization, Writing – original draft, Investigation, Data curation, Writing – review & editing, Supervision. **A. Ciajolo:** Conceptualization, Writing – review & editing, Supervision. **F. Stanzione:** Investigation, Data curation. **A. Tregrossi:** Investigation, Data curation. **B. Apicella:** Conceptualization, Investigation, Data curation, Writing – review & editing, Supervision.

Declaration of competing interest

The authors declare that they have no known competing financial interests or personal relationships that could have appeared to influence the work reported in this paper.

Appendix A. Supplementary data

Supplementary data to this article can be found online at https://doi.org/10.1016/j.carbon.2023.118009.

References

[1] J. Robertson, Photoluminescence mechanism in amorphous hydrogenated carbon, Diam. Relat. Mater. 5 (1996) 457–460, https://doi.org/10.1016/0925-9635(95)00386-X.

[2] P. Desgroux, X. Mercier, K.A. Thomson, Study of the formation of soot and its precursors in flames using optical diagnostics, Proc. Combust. Inst. 34 (2013) 1713–1738, https://doi.org/10.1016/j.proci.2012.09.004.

[3] L.J. Allamandola, A.G. Tielens, J.R. Barker, Interstellar polycyclic aromatic hydrocarbons: the infrared emission bands, the excitation/emission mechanism, and the astrophysical implications, Astrophys. J. Suppl. 71 (1989) 733–775, https://doi.org/10.1086/191396.

[4] X.Y. Xu, R. Ray, Y.L. Gu, H.J. Ploehn, L.- Gearheart, K. Raker, et al., Electrophoretic analysis and purification of fluorescent single-walled carbon nanotube fragments, J. Am. Chem. Soc. 126 (2004) 12736–12737, https://doi.org/10.1021/ja040082h.

[5] N.V. Tepliakov, E.V. Kundelev, P.D. Khavlyuk, Y. Xiong, M.Y. Leonov, W. Zhu, et al., Sp^2–sp^3-hybridized atomic domains determine optical features of Carbon Dots, ACS Nano 13 (2019) 10737–10744, https://doi.org/10.1021/acsnano.9b05444.

[6] M.L. Liu, B.B. Chen, C.M. Li, C.Z. Huang, Carbon dots: synthesis, formation mechanism, fluorescence origin and sensing applications, Green Chem. 21 (2019) 449–471, https://doi.org/10.1039/C8GC02736F.

[7] K.J. Mintz, Y. Zhou, R.M. Leblanc, Recent development of carbon quantum dots regarding their optical properties, photoluminescence mechanism, and core structure, Nanoscale 11 (2019) 4634–4652, https://doi.org/10.1039/C8NR10059D.

[8] M. Fu, F. Ehrat, Y. Wang, K.Z. Milowska, C. Reckmeier, A.L. Rogach, et al., Carbon dots: a unique fluorescent cocktail of polycyclic aromatic hydrocarbons, Nano Lett. 15 (2015) 6030–6035, https://doi.org/10.1021/acs.nanolett.5b02215.

[9] S.N. Baker, G.A. Baker, Luminescent carbon nanodots: emergent nanolights, Angew. Chem., Int. Ed. 49 (2010) 6726–6744, https://doi.org/10.1002/anie.200906623.

[10] H. Li, Z. Kang, Y. Liu, S.-T. Lee, Carbon nanodots: synthesis, properties and applications, J. Mater. Chem. 22 (2012) 24230–24253, https://doi.org/10.1039/C2JM34690G.

[11] R. Wang, K.-Q. Lu, Z.-R. Tang, Y.-J. Xu, Recent progress in carbon quantum dots: synthesis, properties and applications in photocatalysis, J. Mater. Chem. 5 (2017) 3717–3734.

[12] G.A. M Hutton, B.C.M. Martindale, E. Reisner, Carbon dots as photosensitisers for solar-driven catalysis, Chem. Soc. Rev. 46 (2017) 6111–6123, https://doi.org/10.1039/C7CS00235A.

[13] H. Feng, Z. Qian, Functional carbon quantum dots: a versatile platform for chemosensing and biosensing, Chem. Rec. 18 (2018) 491–505, https://doi.org/10.1002/tcr.201700055.

[14] J. Wang, J. Qiu, A review of carbon dots in biological applications, J. Mater. Sci. 51 (2016) 4728–4738, https://doi.org/10.1007/s10853-016-9797-7.

[15] S.Y. Lim, W. Shen, Z. Gao, Carbon quantum dots and their applications, Chem. Soc. Rev. 44 (2015) 362–381, https://doi.org/10.1039/C4CS00269E.

[16] Y. Wang, A. Hu, Carbon quantum dots: synthesis, properties and applications, J. Mater. Chem. C 2 (2014) 6921–6939, https://doi.org/10.1039/c4tc00988f.

[17] D. Reyes, M. Camacho, M. Camacho, M. Mayorga, D. Weathers, G. Salamo, et al., Laser ablated carbon nanodots for light emission, Nanoscale Res. Lett. 11 (2016) 424, https://doi.org/10.1186/s11671-016-1638-8.

[18] Y. Su, M. Xie, X. Lu, H. Wei, H. Geng, Z. Yang, et al., Facile synthesis and photoelectric properties of carbon dots with upconversion fluorescence using arc-synthesized carbon by-products, RSC Adv. 4 (2014) 4839–4842, https://doi.org/10.1039/C3RA45453C.

[19] J. Wang, C.-F. Wang, S. Chen, Amphiphilic egg-derived Carbon Dots: rapid plasma fabrication, pyrolysis process, and multicolor printing patterns, Angew. Chem. Int. Ed. 51 (2012) 9297–9301, https://doi.org/10.1002/anie.201204381.

[20] B. Hu, K. Wang, L. Wu, S.H. Yu, M. Antonietti, M.M. Titirici, Engineering carbon materials from the hydrothermal carbonization process of biomass, Adv. Mater. 22 (2010) 813–828, https://doi.org/10.1002/adma.200902812.

[21] M.M. Titirici, M. Antonietti, Chemistry and materials options of sustainable carbon materials made by hydrothermal carbonization, Chem. Soc. Rev. 39 (2010) 103–116, https://doi.org/10.1039/B819318P.

[22] S.S. Wee, Y.H. Ng, S.M. Ng, Synthesis of fluorescent carbon dots via simple acid hydrolysis of bovine serum albumin and its potential as sensitive sensing probe for lead (II) ions, Talanta 116 (2013) 71–76, https://doi.org/10.1016/j.talanta.2013.04.081.

[23] C. Russo, B. Apicella, A. Ciajolo, Blue and green luminescent carbon nanodots from controllable fuel-rich flame reactors, Sci. Rep. 9 (2019), 14566, https://doi.org/10.1038/s41598-019-50919-1.

[24] M. Sirignano, C. Russo, A. Ciajolo, One-step synthesis of carbon nanoparticles and yellow to blue fluorescent nanocarbons in flame reactors, Carbon 156 (2020) 370–377, https://doi.org/10.1016/j.carbon.2019.09.068.

[25] C. Russo, B. Apicella, A. La Rocca, M. Sirignano, Fluorescent carbon dots synthesis in premixed flames: influence of the equivalence ratio, Carbon 201 (2023) 659–666, https://doi.org/10.1016/j.carbon.2022.09.061.

[26] H.P. Liu, T. Ye, C.D. Mao, Fluorescent carbon nanoparticles derived from candle soot, Angew. Chem., Int. Ed. 46 (2007) 6473–6475, https://doi.org/10.1002/anie.200701271.

[27] H. Zhang, J. liang, J. Liu, S. Chen, H. Zhang, Z. Tian, et al., Monodispersed carbon nanodots spontaneously separated from combustion soot with excitation independent photoluminescence, RSC Adv. 6 (2016) 8456–8460, https://doi.org/10.1039/C5RA20196A.

[28] X. Zhai, P. Zhang, C. Liu, T. Bai, W. Li, L. Dai, et al., Highly luminescent carbon nanodots by microwave-assisted pyrolysis, Chem. Commun. 48 (2012) 7955–7957, https://doi.org/10.1039/C2CC33869F.

[29] D. Saini, Gunture, J. Kaushik, R. Aggarwal, K.M. Tripathi, S.K. Sonkar, Carbon nanomaterials derived from black carbon soot: a review of materials and applications, ACS Appl. Nano Mater. 4 (12) (2021) 12825–12844, https://doi.org/10.1021/acsanm.1c02840.

[30] P. Kumar, H.B. Bohidar, Observation of fluorescence from non-functionalized carbon nanoparticles and its solvent dependent spectroscopy, J. Lumin. 141 (2013) 155–161, https://doi.org/10.1016/j.jlumin.2013.02.043.

[31] X. Xu, R. Ray, Y. Gu, H.J. Ploehn, L. Gearheart, K. Raker, et al., Electrophoretic analysis and purification of fluorescent single-walled carbon nanotube fragments, J. Am. Chem. Soc. 126 (2004) 12736–12737, https://doi.org/10.1021/ja040082h.

[32] Y.-P. Sun, B. Zhou, Y. Lin, W. Wang, K.A.S. Fernando, P. Pathak, et al., Quantum-sized carbon dots for bright and colorful photoluminescence, J. Am. Chem. Soc. 128 (2006) 7756–7757, https://doi.org/10.1021/ja062677d.

[33] C. Russo, A. Carpentieri, A. Tregrossi, A. Ciajolo, B. Apicella, Blue, green and yellow carbon dots derived from pyrogenic carbon: structure and fluorescence behaviour, Carbon 201 (2023) 900–909, https://doi.org/10.1016/j.carbon.2022.09.062.
[34] J.B. Essner, J.A. Kist, L. Polo-Parada, G.A. Baker, Artifacts and errors associated with the ubiquitous presence of fluorescent impurities in carbon nanodots, Chem. Mater. 30 (2018) 1878–1887, https://doi.org/10.1021/acs.chemmater.7b04446.
[35] C.M. Carbonaro, R. Corpino, M. Salis, F. Mocci, S.V. Thakkar, C. Olla, et al., On the emission properties of carbon dots: reviewing data and discussing models, J Carbon research C 5 (2019) 60, https://doi.org/10.3390/c5040060.
[36] S. Zhu, Y. Song, X. Zhao, J. Shao, J. Zhang, B. Yang, The photoluminescence mechanism in Carbon Dots (Graphene Quantum Dots, carbon nanodots, and polymer dots): current state and future perspective, Nano Res. 8 (2015) 355–381, https://doi.org/10.1007/s12274-014-0644-3.
[37] H. Ding, S.B. Yu, J.S. Wei, H.M. Xiong, Full-color light-emitting Carbon Dots with a surface-state-controlled luminescence mechanism, ACS Nano 10 (2016) 484–491, https://doi.org/10.1021/acsnano.5b05406.
[38] K.J. Mintz, Y. Zhou, R.M. Leblanc, Recent development of carbon quantum dots regarding their optical properties, photoluminescence mechanism, and core structure, Nanoscale 11 (2019) 4634–4652, https://doi.org/10.1039/C8NR10059D.
[39] H.J. Yoo, B.E. Kwak, D.H. Kim, Competition of the roles of π-conjugated domain between emission center and quenching origin in the photoluminescence of carbon dots depending on the interparticle separation, Carbon 183 (2021) 560–570, https://doi.org/10.1016/j.carbon.2021.07.054.
[40] J. Schneider, C.J. Reckmeier, Y. Xiong, M. von Seckendorff, A.S. Susha, P. Kasak, et al., Molecular fluorescence in citric acid-based Carbon Dots, J. Phys. Chem. C 121 (2017) 2014–2022, https://doi.org/10.1021/acs.jpcc.6b12519.
[41] W. Kasprzyk, T. Swiergosz, S. Bednarz, K. Walas, N.V. Bashmakova, D. Bogdał, Luminescence phenomena of carbon dots derived from citric acid and urea - a molecular insight, Nanoscale 10 (2018) 13889–13894, https://doi.org/10.1039/C8NR03602K.
[42] F. Yan, Z. Sun, H. Zhang, X. Sun, Y. Jiang, Z. Bai, The fluorescence mechanism of carbon dots, and methods for tuning their emission color: a review, Microchim. Acta 186 (2019) 583, https://doi.org/10.1007/s00604-019-3688-y.
[43] Y. Xiong, J. Schneider, E.V. Ushakova, A.L. Rogach, Influence of molecular fluorophores on the research field of chemically synthesized carbon dots, Nano Today 23 (2018) 124–139, https://doi.org/10.1016/j.nantod.2018.10.010.
[44] W. Kasprzyk, T. Swiergosz, S. Bednarz, K. Walas, N.V. Bashmakova, D. Bogdał, Luminescence phenomena of carbon dots derived from citric acid and urea - a molecular insight, Nanoscale 10 (2018) 13889–13894, https://doi.org/10.1039/C8NR03602K.
[45] K.J. Mintz, M. Bartoli, M. Rovere, Y. Zhou, S.D. Hettiarachchi, S. Paudyal, et al., A deep investigation into the structure of carbon dots, Carbon 173 (2021) 433–447, https://doi.org/10.1016/j.carbon.2020.11.017.
[46] M. Righetto, F. Carraro, A. Privitera, G. Marafon, A. Moretto, C. Ferrante, The elusive nature of Carbon Nanodot fluorescence: an unconventional perspective, J. Phys. Chem. C 124 (2020) 22314–22320, https://doi.org/10.1021/acs.jpcc.0c06996.
[47] F. de Andres, A. Ríos, Carbon dots – separative techniques: tools-objective towards green analytical nanometrology focused on bioanalysis, Microchem. J. 161 (2021), 105773, https://doi.org/10.1016/j.microc.2020.105773.
[48] V. Hinterberger, C. Damm, P. Haines, D.M. Guldi, W. Peukert, Purification and structural elucidation of carbon dots by column chromatography, Nanoscale 11 (2019) 8464, https://doi.org/10.1039/C9NR01029G.
[49] C.-Y. Chen, Y.-H. Tsai, C.-W. Chang, Evaluation of the dialysis time required for carbon dots by HPLC and the properties of carbon dots after HPLC fractionation, New J. Chem. 43 (2019) 6153, https://doi.org/10.1039/C9NJ00434C.
[50] B. Apicella, M. Millan, A.A. Herod, A. Carpentieri, P. Pucci, A. Ciajolo, Separation and measurement of flame-formed high molecular weight polycyclic aromatic hydrocarbons by size-exclusion chromatography and laser desorption/ionization time-of-flight mass spectrometry, Rapid Commun. Mass Spectrom. 20 (2006) 1104–1108, https://doi.org/10.1002/rcm.2419.
[51] J.C. Vinci, I.M. Ferrer, S.J. Seedhouse, A.K. Bourdon, J.M. Reynard, B.A. Foster, et al., Hidden properties of Carbon Dots revealed after HPLC fractionation, J. Phys. Chem. Lett. 4 (2013) 239–243, https://doi.org/10.1021/jz301911y.
[52] F. Ehrat, S. Bhattacharyya, J. Schneider, A. Lof, R. Wyrwich, A.L. Rogach, et al., Tracking the source of Carbon Dot photoluminescence: aromatic domains versus molecular fluorophores, Nano Lett. 17 (2017) 7710–7716, https://doi.org/10.1021/acs.nanolett.7b03863.
[53] B. Apicella, R. Barbella, A. Ciajolo, A. Tregrossi, Formation of low- and high-molecular-weight hydrocarbon species in sooting ethylene flames, Combust. Sci. Technol. 174 (2002) 309–324, https://doi.org/10.1080/713712948.
[54] C. Russo, B. Apicella, A. Tregrossi, M.M. Oliano, A. Ciajolo, Thermophoretic sampling of large PAH (C≥[22–24]) formed in flames, Fuel 263 (2020), 116722, https://doi.org/10.1016/j.fuel.2019.116722.
[55] C. Russo, A. Ciajolo, F. Stanzione, A. Tregrossi, M.M. Oliano, A. Carpentieri, et al., Investigation on chemical and structural properties of coal- and petroleum-derived pitches and implications on physico-chemical properties (solubility, softening and coking), Fuel 245 (2019) 478–487, https://doi.org/10.1016/j.fuel.2019.02.040.
[56] C. Russo, A. Tregrossi, A. Ciajolo, Dehydrogenation and growth of soot in premixed flames, Proc. Combust. Inst. 35 (2015) 1803–1809, https://doi.org/10.1016/j.proci.2014.05.024.
[57] C. Russo, F. Stanzione, A. Tregrossi, A. Ciajolo, Infrared spectroscopy of some carbon-based materials relevant in combustion: qualitative and quantitative analysis of hydrogen, Carbon 74 (2014) 127–138, https://doi.org/10.1016/j.carbon.2014.03.014.
[58] B. Apicella, R. Barbella, A. Ciajolo, A. Tregrossi, Comparative analysis of the structure of carbon materials relevant in combustion, Chemosphere 51 (2003) 1063–1069, https://doi.org/10.1016/S0045-6535(02)00715-4.
[59] C. Russo, F. Stanzione, A. Ciajolo, A. Tregrossi, Study on the contribution of different molecular weight species to the absorption UV–Visible spectra of flame-formed carbon species, Proc. Combust. Inst. 34 (2013) 3661–3668, https://doi.org/10.1016/j.proci.2012.06.097.
[60] J. Tauc, R. Grigorovici, A. Vancu, Optical properties and electronic structure of amorphous germanium, Phys. Status Solidi B 15 (1966) 627–637, https://doi.org/10.1002/pssb.19660150224.
[61] J. Robertson, E.P. O'Reilly, Electronic and atomic structure of amorphous carbon, Phys. Rev. B 35 (1987) 2946–2957, https://doi.org/10.1103/PhysRevB.35.2946.
[62] I.B. Berlman, Handbook of Fluorescence Spectra of Aromatic Molecules, Academic Press, New York, 1971.
[63] B. Apicella, C. Russo, A. Carpentieri, A. Tregrossi, A. Ciajolo, PAHs and fullerenes as structural and compositional motifs tracing and distinguishing organic carbon from soot, Fuel 309 (2022), 122356, https://doi.org/10.1016/j.fuel.2021.122356.
[64] C. Russo, B. Apicella, J.S. Lighty, A. Ciajolo, A. Tregrossi, Optical properties of organic carbon and soot produced in an inverse diffusion flame, Carbon 124 (2017) 372–379, https://doi.org/10.1016/j.carbon.2017.08.073.
[65] S.H. Ko, T. Lee, H. Park, D.S. Ahn, K. Kim, Y. Kwon, et al., Nanocage-confined synthesis of fluorescent polycyclic aromatic hydrocarbons in zeolite, J. Am. Chem. Soc. 140 (2018) 7101–7107, https://doi.org/10.1021/jacs.8b00900.
[66] A. Keller, R. Kovacs, K.H. Homann, Large molecules, ions, radicals and small soot particles in fuel-rich hydrocarbon flames, Part IV. Large polycyclic aromatic hydrocarbons and their radicals in a fuel-rich benzene-oxygen flame, Phys. Chem. Chem. Phys. 2 (2000) 1667–1675, https://doi.org/10.1039/A908190I.
[67] J. Robertson, Recombination and photoluminescence mechanism in hydrogenated amorphous carbon, Phys. Rev. B 53 (1996) 16302–16305, https://doi.org/10.1103/physrevb.53.16302.
[68] I. Llamas-Jansa, C. J€ager, H. Mutschke, Th Henning, Far-ultraviolet to near infrared optical properties of carbon nanoparticles produced by pulsed-laser pyrolysis of hydrocarbons and their relation with structural variations, Carbon 45 (2007) 1542–1557, https://doi.org/10.1016/j.carbon.2007.02.032.
[69] A. Menon, J.A. Dreyer, J.W. Martin, J. Akroyd, J. Robertson, M. Kraft, Optical band gap of cross-linked, curved, and radical polyaromatic hydrocarbons, Phys. Chem. Chem. Phys. 21 (2019) 16240–16251, https://doi.org/10.1039/C9CP02363A.
[70] C. Russo, B. Apicella, A. Tregrossi, A. Ciajolo, K.C. Le, S. Török, et al., Optical band gap analysis of soot and organic carbon in premixed ethylene flames: comparison of in-situ and ex-situ absorption measurements, Carbon 158 (2020) 89–96, https://doi.org/10.1016/j.carbon.2019.11.087.
[71] R.L. Vander Wal, Soot precursor material: visualization via simultaneous lIF-LII and characterization via tem, Symposium (International) on Combustion 26 (1996) 2269–2275, https://doi.org/10.1016/S0082-0784(96)80054-3.